Journal of Cerebral Blood Flow & Metabolism (2015) 35, 1331–1338

www.jcbfm.com

ORIGINAL ARTICLE

[^{11}C]PBR28 PET imaging is sensitive to neuroinflammation in the aged rat

Matthew D Walker[1,5], Katherine Dinelle[2], Rick Kornelsen[2], Nathan V Lee[2], Qing Miao[3], Mike Adam[3], Christine Takhar[3], Edwin Mak[2], Michael Schulzer[2], Matthew J Farrer[4] and Vesna Sossi[1]

Neuroinflammation in the aging rat brain was investigated using [^{11}C]PBR28 microPET (positron emission tomography) imaging. Normal rats were studied alongside LRRK2 p.G2019S transgenic rats; this mutation increases the risk of Parkinson's disease in humans. Seventy [^{11}C]PBR28 PET scans were acquired. Arterial blood sampling enabled tracer kinetic modeling and estimation of V_T. *In vitro* autoradiography was also performed. PBR28 uptake increased with age, without differences between nontransgenic and transgenic rats. In 12 months of aging (4 to 16 months), standard uptake value (SUV) increased by 56% from 0.44 to 0.69 g/mL, whereas V_T increased by 91% from 30 to 57 mL/cm^3. Standard uptake value and V_T were strongly correlated ($r = 0.52$, 95% confidence interval (CI) = 0.31 to 0.69, $n = 37$). The plasma free fraction, f_p, was 0.21 ± 0.03 (mean ± standard deviation, $n = 53$). *In vitro* binding increased by 19% in 16 months of aging (4 to 20 months). The SUV was less variable across rats than V_T; coefficients of variation were 13% ($n = 27$) and 29% ($n = 12$). The intraclass correlation coefficient for SUV was 0.53, but was effectively zero for V_T. These data show that [^{11}C]PBR28 brain uptake increases with age, implying increased microglial activation in the aged brain.

Journal of Cerebral Blood Flow & Metabolism (2015) **35,** 1331–1338; doi:10.1038/jcbfm.2015.54; published online 1 April 2015

Keywords: LRRK2; microPET; neuroinflammation; Parkinson's disease; PBR28; TSPO

INTRODUCTION

Neuroinflammation is known to be present in a variety of neurologic diseases, including Alzheimer's disease and Parkinson's disease (PD). The role of neuroinflammation in these diseases remains uncertain, but there is evidence that neuroinflammation may drive some pathologic processes in the diseased brain.[1–3] The study of neuroinflammation in rodent models may prove enlightening, furthering our understanding of how neuroinflammation is implicated in the pathogenesis of neurodegenerative diseases and allowing therapies that target pathologic aspects of neuroinflammation to be tested. This is especially the case when measurements can be made non-invasively and longitudinally via neuroimaging. Such investigations should be preceded by the examination of neuroinflammation in normal aging, as longevity is the single greatest risk factor for common neurodegenerative diseases.

[^{11}C]PBR28 is a recently developed positron emission tomography (PET) tracer designed for imaging inflammation.[4] This report details results obtained from [^{11}C]PBR28 PET imaging of the rat brain across a wide age range. The study was preceded by a basic validation of the methods in unilaterally 6-hydroxydopamine (6-OHDA) lesioned rats, where we obtained good agreement between [^{11}C]PBR28 PET and autoradiography.[5] We then imaged young and aged rats to assess the effect of aging on [^{11}C]PBR28 brain uptake. Measurements were performed in both normal control and transgenic rats that overexpress a mutated form of LRRK2, known to increase the risk of PD in human carriers.[6,7] In all study groups, PET imaging was complemented by *in vitro* [^{11}C]PBR28 autoradiography.

The radiotracer [^{11}C]PBR28 is a second-generation ligand for the 18-kDa translocator protein (TSPO), formerly known as the peripheral benzodiazepine receptor (PBR). Translocator protein is predominantly found on the outer mitochondrial membrane.[8] Although widely expressed in the body, central expression of TSPO is mainly restricted to ependymal and glial cells.[9,10] Activated microglia have an increased TSPO expression.[11] Increased central binding of TSPO ligands such as PBR28 can normally be ascribed to microglial activation, a hallmark of chronic neuroinflammation and also present after acute insults that evoke inflammatory responses.

Several reports describe the results from microPET imaging using [^{11}C]PBR28.[4,12,13] There is also a large literature concerning the application of other TSPO ligands in the study of neuroinflammation in rodents using PET (and many others).[14,15] Increases were observed in the uptake of the first-generation TSPO ligand [^{11}C](R)-PK11195 with age in a transgenic mouse model of Alzheimer's disease.[16] Similarly, increases were observed in the uptake of the second-generation TSPO ligand [^{18}F]DPA-714 with age, in corpulent rats.[17]

Aging leads to an increase in the number of activated microglia in the rat brain, without a concomitant increase in the total number of microglia as determined by Ogura *et al*[18] via

[1]Department of Physics and Astronomy, University of British Columbia, Vancouver, British Columbia, Canada; [2]Pacific Parkinson's Research Centre, University of British Columbia, Vancouver, British Columbia, Canada; [3]TRIUMF, Vancouver, British Columbia, Canada and [4]Department of Medical Genetics, Centre for Applied Neurogenetics, University of British Columbia, Vancouver, British Columbia, Canada. Correspondence: Dr MD Walker, Department of Medical Physics and Clinical Engineering, Churchill Hospital, Oxford University Hospitals NHS Trust, Oxford OX3 7LE, UK.
E-mail: matthew.walker@ouh.nhs.uk
[5]Current Address: Oxford University Hospitals NHS Trust, Oxford OX3 7LE, UK.
The research was supported by the Michael J Fox Foundation for Parkinson's Research (VS), the Canadian Institutes of Health Research grant FRN: MFE 123709 (MDW), the NSERC (VS), and the Canada Excellence Research Chair (MJF) program.
Received 29 August 2014; revised 28 January 2015; accepted 9 March 2015; published online 1 April 2015

immunohistochemical staining. We hence predict an increase in TSPO expression in the aging brain. Since microglial expression of TSPO is influenced by the degree of activation,[15] the increased TSPO expression may differ from the relative increase in the number of activated microglia, perhaps with important implications for the aging brain. We hypothesized that TSPO expression would increase more rapidly and by a greater amount in the case of LRRK2 p.G2019S transgenic rats compared with wild-type rats, because evidence suggests that mutations in LRRK2 can lead to exacerbated neuroinflammation.[19,20]

MATERIALS AND METHODS

Animal Procedures

Procedures involving animals were approved by the University of British Columbia's ethics committee and performed in accordance with the Canadian Council on Animal Care guidelines. For assessment of aging effects, we used male Sprague Dawley rats alongside male hemizygous BAC LRRK2 p.G2019S rats. These transgenic rats have some behavioral deficits but do not have overt dopaminergic degeneration or dysfunction.[21] Some of these rats underwent intraperitoneal injection of saline when aged 4 months, but this was assumed not to affect PBR28 uptake in the brain. The animals were maintained in controlled standard conditions of temperature (21°C) and humidity, on a 12-hour light cycle (light from 0700 to 1900 hours). Water was available *ad libitum*, while a mild food restriction (50 g of chow per day; 60 g/day for rats weighing over 825 g) started at 3 months of age.

Radiotracer Synthesis

The synthesis of [^{11}C]PBR28 followed a procedure modified from that of Hoareau *et al*.[22] Briefly, the desmethyl precursor was allowed to react with [^{11}C]methyl iodide in *N*,*N*-dimethylformamide in an automated synthesizer (Tacerlab FXc-Pro; GE Healthcare, Waukesha, WI, USA). The crude produce was purified by HPLC (high performance liquid chromatography), followed by solid-phase extraction (C-18 SepPak; Waters, Milford, MA, USA) and elution of the final product with an ethanol solution.

The specific activity at the time of injection was 112 ± 54 GBq/μmol (mean ± s.d.). The injected activity was 45 ± 1 MBq/kg body weight, with the injected mass being 0.53 ± 0.36; 0.18 to 2.6 nmol/kg (mean ± s.d.; range).

[^{11}C]PET28 Positron Emission Tomography Imaging

To assess aging effects, [^{11}C]PBR28 PET imaging was performed in 44 male rats, of which 25 were transgenic and 19 were nontransgenic. A total of 70 scans were performed, with each rat being scanned on 1 to 3 occasions. In two aged male transgenic rats, we performed presaturation studies to ascertain the extent to which V_T comprises displaceable binding. In these studies, imaging was performed 25 to 30 minutes after intravenous injection of 10 mg/kg body weight PK11195 (Abcam Inc., Cambridge, UK). This relatively high dose of PK11195 (10 mg/kg) allows direct comparison with the results of Imaizumi *et al*.[12] In the first rat, this was dissolved in 1 mL of DMSO. Following concerns over potential physiologic effects when using this volume of DMSO,[23] we reduced the volume to 0.5 mL for the second rat.

On a separate occasion these two rats were imaged after injection of the vehicle only (DMSO; 0.5 or 1 mL as above). The second rat was also imaged under baseline conditions.

The MicroPET Focus120 small animal scanner (Concorde/Siemens, Knoxville, TN, USA) was used.[24] Animals were anesthetized using 2.5% isoflurane during scanning. Their heart rate and blood oxygen saturation level were monitored using a pulse oximeter, and their temperature was monitored using a digital thermometer and maintained at 35°C to 36°C using a heat lamp. Respiration was visually monitored. Ear bars were used to immobilize the head and provide accurate positioning of the brain at the center of the scanner. After acquisition of a 10-minute ^{57}Co transmission scan, the radiotracer was injected as a 30-second bolus, intravenously at the tail using a 25-gauge, 19-mm long catheter (BD Insyte; Becton, Dickinson and Co., Franklin Lakes, NJ, USA). Emission data were then collected for 90 minutes in listmode. These data were fully corrected for randoms, attenuation, scatter, normalization, and dead time. After Fourier rebinning, images were reconstructed using 2D filtered back-projection, calibrated, and decay corrected. The spatial resolution of this system is < 1.5 mm FWHM (full width at half maximum).[24]

In 43 of the 70 scans, a 25-gauge, 19-mm long catheter (BD Insyte) was placed into the ventral artery of the tail immediately before the PET scan.[25] Arterial blood samples were manually collected immediately after completion of the tracer injection. Rapid sampling in the first 2.5 minutes of the scan provided four samples on average, followed by samples at 3, 4, 5.5, 7, 10, 20, 45, and 70 minutes; accurate measurement and automated recording of the collection times was achieved using a foot-pedal system. Blood from the tubing dead space was discarded. The collected volume was 50 to 100 μL per sample. In 2 scans arterial catheterization was not attempted, and in 25 scans the arterial catheterization failed (average catheterization success rate of 63% over the full course of the study; approximately 90% by the study end). When arterial catheterization failed, venous blood was collected from the tail (opposite side to tracer injection).

Blood Processing During [^{11}C]PET28 Positron Emission Tomography

Blood samples were centrifuged for 2 minutes at 16,100 *g*. The arterial plasma was then drawn off by pipette and its activity measured in an automated well counter (Cobra II Auto Gamma Counter, Packard Instrument Co., Meriden, CT, USA). The samples collected at 2, 4, 7, 10, 20, and 45 minutes were further processed for analysis of radiolabelled metabolites via HPLC. The plasma was mixed 1:1 in acetonitrile (Fisher Scientific, Pittsburgh, PA, USA) to precipitate protein from the sample, and centrifuged for 5 minutes at 16,100 *g*. The supernatant was then injected onto the HPLC system, with minimal activity left in the protein pellet. The system comprises a pump (model 600E; Waters), manual injector (Rheodyne, Rohnert Park, CA, USA) with 2.4 mL loop, dual-wavelength absorbance detector (Model 2487, Waters), a lead-shielded radiation detector (model FC-3200; Bioscan, Washington, DC, USA) and a fraction collector (model 203B; Gilson, Middleton, WI, USA). A 250-mm long, 10-mm diameter Luna 5 μm C18(2) 100 Å column was used (Phenomenex, Torrance, CA, USA) with guard column (10 mm long, 10 mm diameter, SecurityGuard SemiPrep; Phenomenex). Mobile phase consisted of 62% acetonitrile and 38% ammonium acetate (0.1 mol/L). The flow rate was 4.0 mL/min. Ten 1-minute fractions were collected and measured using a well counter (as previous), from which the unchanged PBR28 fraction was calculated.

The tracer's free fraction (f_p) in plasma was measured in 53 studies. The measurement was performed in duplicate or triplicate depending on the total plasma volume available, derived from arterial or venous blood. Plasma (approximately 500 μL for duplicate measurements; 750 μL for triplicate) was spiked with 0.1 MBq of [^{11}C]PBR28 (typical volume 15 μL; $< 10\%$ total plasma volume). The sample was then briefly vortexed and incubated at room temperature for 10 minutes. In all, 150 μL of the sample was then placed in each of the two or three ultrafiltration devices (Centrifree Ultrafiltration Device with Ultracel YM-T membrane; EMD Millipore, Billerica, MA, USA). The activity concentration in the sample was determined by measurement of an aliquot (~50 μL) in a well counter (as previous). The ultrafiltration devices were spun for 15 minutes at room temperature at 2,000 g. The activity in 75 μL of the sample filtrate was then measured in a well counter (as previous). In parallel to this, the same procedure was performed using the same volume of phosphate-buffered saline. The plasma-free fraction was calculated as the ratio of activities (after correcting for decay) between the plasma filtrate and the spiked plasma, increased by correcting for the fraction of activity retained in the ultrafiltration device found for phosphate-buffered saline.

[^{11}C]PBR28 Positron Emission Tomography Image Analysis

A [^{11}C]PBR28 rat brain template was generated by coregistration of six such scans to the cryo-image of Rubins *et al*.[26] The template was then coregistered to each of the [^{11}C]PBR28 images in this study. The same transformation was applied to an eroded version of the corresponding brain atlas.[26] Erosion of the atlas reduced the region sizes with the aim of reducing partial volume errors and errors from misregistration. The atlas contained six regions (cerebellum, cortex, thalamus, striatum, hippocampus, and other) that were combined to form an addition region (whole brain). The dynamic PET images were sampled using these regions and the resulting time-activity curves were used to calculate: (1) the standard uptake value (SUV; g/mL) between 45 and 90 minutes post injection and (2) the volume of distribution (V_T) of the tracer in brain tissue compared with arterial plasma. In the case of SUV, we used the definition of average activity concentration for the region and time window (kBq/mL), divided by the injected activity per unit body weight (MBq/kg). Two methods were used to estimate V_T, both of which used the metabolite-corrected arterial

plasma input function. First, the graphical method of Logan *et al*[27] was used, fitting data between 10 and 65 minutes without correction for blood volume. Second, we applied a standard two-tissue compartmental model using unconstrained nonlinear least squares (NLLS) fitting with weights similar to those described previously,[28] and assuming a 5% blood volume. Nonlinear least squares provided estimates of four rate constants (K_1, k_2, k_3, k_4), from which the binding potential (BP_{ND})[29] was calculated ($BP_{ND} = k_3/k_4$) as well as the volume of distribution, $V_T = (K_1/k_2) \times (1+k_3/k_4)$. The standard errors on the rate constants, V_T, and BP_{ND} were calculated from the covariance matrix.[30]

In vitro [^{11}C]PBR28 Autoradiography

Animals were killed by decapitation. The brain was rapidly extracted and flash-frozen using isopentane and dry ice before being stored at −80°C. Using a microtome cryostat (HM 500 OM; Microm International, Walldorf, Germany), sagittal sections were cut at 16 μm and electrostatically adhered to glass microscope slides (Fisherbrand Superfrost Plus; Fisher Scientific) before being dried and stored at −80°C. *In vitro* [^{11}C]PBR28 autoradiography made use of an incubation buffer of 50 mmol/L Tris-HCl pH 7.8, 50 mmol/L NaCl, 3 mmol/L EDTA. [^{11}C]PBR28 (2 nmol/L) was added to this buffer and slices were incubated at room temperature for 30 minutes. An ice-cold (4°C) rinsing buffer of 10 mmol/L Tris-HCl pH 7.4, 150 mmol/L NaCl was then used, with 5 washes each lasting 1 minute. Slides from adjacent sections were incubated in parallel, using the same buffer but with the addition of nonradioactive PK11195 (1 μmol/L; Abcam Inc.) to measure nonspecific binding. After incubation, the slides were dried and placed on a phosphor screen (multisensitive imaging plate; Perkin-Elmer, Waltham, MA, USA), alongside standards of eight different ^{11}C activity concentrations to allow accurate quantification over a wide range. After exposure, the screen was read using a high-resolution phosphor imager (cyclone storage phosphor system; Packard Bioscience Co., Meriden, CT, USA). The spatial resolution of this system is approximately 470 μm.[31] Regions of interest were positioned on autoradiography slices using the manufacturer's software (OptiQuant; Parkard Instrument Co.). Regions included the striatum (4.7 mm^2), frontal cortex (6.5 mm^2), cerebellum (15.5 mm^2), and midbrain (6.3 mm^2). These four regions were combined to form the whole-brain region (33 mm^2) used for primary analysis. Regions were also placed on the eight ^{11}C standards, from which a calibration line was derived for conversion of the measured signal (OptiQuant digital light units (DLU)) into activity (Bq) at the reference time. The concentration of bound ligand (pmol/cc) in each region was then estimated by quantifying the DLU per unit area, subtracting the contribution from nonspecific binding (typically $<$ 10% of the total), dividing by the slice thickness to calculate the DLU per unit volume, converting to an activity concentration using the aforementioned calibration factor, and then dividing by the specific activity at the reference time.

Statistical Analysis

Statistical analyses were performed using Matlab 7.11.0 (The Mathworks, Inc., Natick, MA, USA). Several models were considered to describe the dependencies of the whole-brain SUV and whole-brain V_T on age, including polynomial, exponential, and logarithmic functions. The most appropriate model was selected by consideration of the residual variance and the significance level of the coefficients. In both cases, the selected model was a polynomial of the form:

$$y = a_0 + a_1 x + a_2 x^2, \quad (1)$$

where x is age (days) and y is the measure of tracer uptake, either the SUV (g/mL) or V_T (mL/cm^3). The significance levels for inclusion of a genotype term in the age model, and the genotype × age, and genotype × age^2 interactions were calculated along with the 95% confidence interval for the model fit.

For a robust and simple measure of the dependence of SUV on age for brain subregions, which yielded more variable data compared with the whole brain, we used the slope from a linear regression between the regional SUV and age.

To assess the repeatability of the measurements, the intraclass correlation coefficient (ICC) was calculated using the residual differences from the age-relationship model, using data from rats for which two repeated measurements were available. In the few rats that had three measurements available, we selected the two scans performed closest together in time for the repeatability analysis. Twelve pairs of scans were used to calculate the ICC for the SUV, and eight pairs for V_T's ICC. The average time between the paired measurements was 91 days. We also calculated the coefficient of variation (CoV = standard deviation/mean) for the SUV, V_T, and V_T/f_p measurements using data from rats aged 3.9 months (age range = 3.4 to 4.4 months; $n = 27$, 12, and 12, respectively), without applying any correction for aging effects.

To assess the extent to which changes in V_T were mirrored by changes in SUV, we performed a linear regression between these two variables. The strength of the correlation was quantified by Pearson's correlation coefficient (r). The 95% confidence interval (CI) for r was estimated by bootstrap resampling (basic percentile method). In addition, we assessed the correlation between the residuals, from their respective age-relationship models, for SUV and V_T. This was achieved by performing linear regression on the residual differences from the respective aging models, and allowed us to ascertain whether 'basal' variations in SUV and V_T, i.e., those that occur in the absence of age differences, are correlated.

Results from autoradiography were primarily assessed using the whole-brain region, by performing a two-way analysis of variance with factors being genotype and age. This was followed by repetition of the analysis for the various subregions. No *post hoc* testing was performed.

RESULTS

Imaging Characteristics

High-resolution autoradiography resolved the binding of the compound to the lining of the ventricular system (to the TSPO-rich ependymal cells). When viewed using PET, much of the ventricular system appears as an area of high uptake with no distinction between the lining of the ventricles and the cerebrospinal fluid contained within them. Example PET and autoradiography images, taken from our initial study[5] in which unilateral 6-OHDA lesioning provided a positive control,[32] are displayed in Figure 1.

PBR28 Blood Measurements

Arterial blood sampling enabled measurement of [^{11}C]PBR28 metabolism and the total activity concentration in arterial plasma, from which the arterial input function is calculated. These data are shown in Figure 2. The metabolism of [^{11}C]PBR28 occurs rapidly in the rat, with 50% of the radioactivity in arterial blood consisting of the parent compound at 6.5 minutes after injection, reducing to 10% at 45 minutes. The variability on the presented group data in Figure 2 relates to real variability across rats, since the individual rats' blood data typically followed smooth curves that were distinct from that found in others rats. Some measurements of metabolism were also made using venous blood collected from the tail, but these were highly variable between rats, did not resemble the measurements made using arterial blood, provided substantially higher unchanged fractions, and were not deemed useful for kinetic modeling.

The tracer's free fraction in plasma, measured at the time of 53 PET scans using ultrafiltration, was 0.21 ± 0.03 (mean, s.d.). The data were assessed for any dependence on genotype (normal control versus transgenic), blood sample type (venous versus arterial), and the animal's age. There was no suggestion that any of these factors influenced the measurement as determined by analysis of covariance.

Blood and Blood-Free Quantification of PBR28 Brain Uptake

There was a reasonable correlation between the tracer uptake estimated using V_T (with arterial blood input and Logan graphical analysis) and the SUV. This relationship is shown for 37 scans in Figure 3C. Pearson's correlation coefficient was 0.52 and highly significant (95% CI = 0.31 to 0.69). Regression of the residual differences from the aging model for SUV with the residuals for V_T provided a week, nonsignificant correlation ($r = 0.17$, $P = 0.29$).

V_T estimated by Logan graphical analysis was very highly correlated with V_T estimated by NLLS fitting. An example fit for both methods is shown in Figure 3. Linear regression provided the relationship $V_{T(logan)} = 0.92\, V_{T(NLLS)} + 2.0$, $r = 0.99$, where the slope

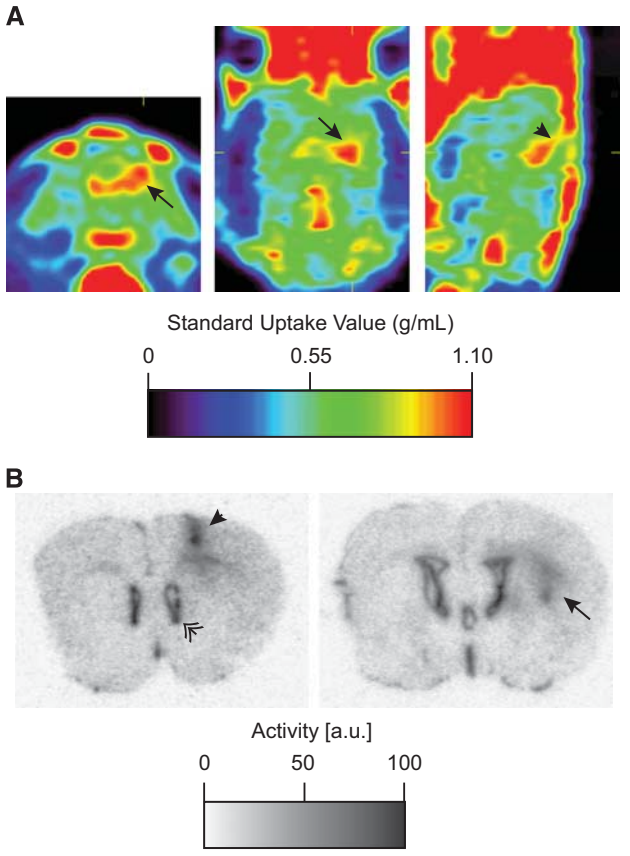

Figure 1. Example [^{11}C]PBR28 positron emission tomography (PET) and [^{11}C]PBR28 *in vitro* autoradiography images taken from our initial validation study in 6-hydroxydopamine (6-OHDA) lesioned rats.[5] (**A**) PET images (a coronal, horizontal, and saggital section through the striatum). (**B**) Autoradiography images (coronal sections through the striatum). Increased tracer uptake in the lesioned (right) striatum is shown by the arrow. An area of increased binding shown by the solid arrowhead follows the needle tract. Both were clearly observed on many adjacent autoradiography slices. Binding to the ependyma is also observed, shown by the double-headed arrowhead. PET imaging took place 3 days after injection of 10 μg 6-OHDA into the right striatum, and the rat was killed the following day. The hemisphere contralateral to the lesion is representative of normal control rats.

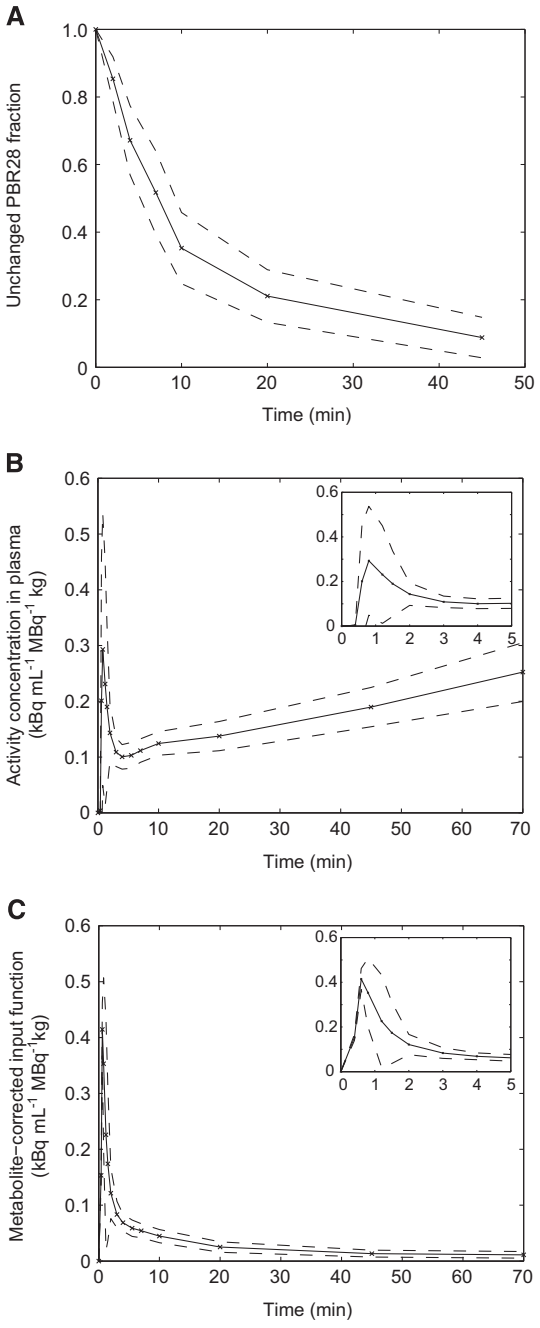

Figure 2. Arterial blood data collected during [^{11}C]PBR28 positron emission tomography (PET) scanning. (**A**) Unchanged fractions showing [^{11}C]PBR28 metabolism. (**B**) Total activity concentration in plasma, normalized by the injected dose per unit body weight. (**C**) Arterial input function, normalized by the injected dose per unit body weight. In all cases, the dashed lines are at ± 1 standard deviation from the mean. Insets in (**B**) and (**C**) show a close-up of the first 5 minutes.

was lower than 1 primarily due to inclusion of the blood volume in NLLS. In many cases (17/37) BP_{ND} was not identifiable using NLLS (standard errors $>20\%$), but in the remaining data ($n=20$) we found a linear relationship between BP_{ND} and V_T ($BP_{ND}=0.084\,V_T+0.51$, $r=0.61$, $P=0.004$). There was no dependence of K_1/k_2 on age in this reduced data set, whereas BP_{ND} increased with age ($P<0.01$).

The ICC for SUV was 0.525 (95% CI: 0 to 0.83). For V_T, the ICC was effectively zero, indicating that measurement errors in V_T are much larger than true variations in V_T across the sample population. The coefficient of variation for SUV, V_T, and V_T/f_p in 4-month-old rats was 13%, 29%, and 38%.

PBR28 Binding in the Brain Increases with Age

Table 1 lists the binding measurements of [^{11}C]PBR28 in various brain structures, as determined by autoradiography in young (4.0 months) and aged (19.6 months) rats. These measurements showed a 19% increase in the expression of TSPO with aging, with the increase being statistically significant (whole-brain region; age: $P=0.044$; genotype: $P=0.23$). In the analysis of autoradiography subregions, aging effects were significant for the cerebellum and the striatum. In all cases, there were no significant genotype effects or significant genotype $\times$ age interactions.

[^{11}C]PBR28 PET imaging also found a significant age-related increase, but here the fractional increases were larger as shown in Figure 4. The PET-derived SUV and V_T significantly increased with age ($P<0.001$), without any significant effect of genotype and

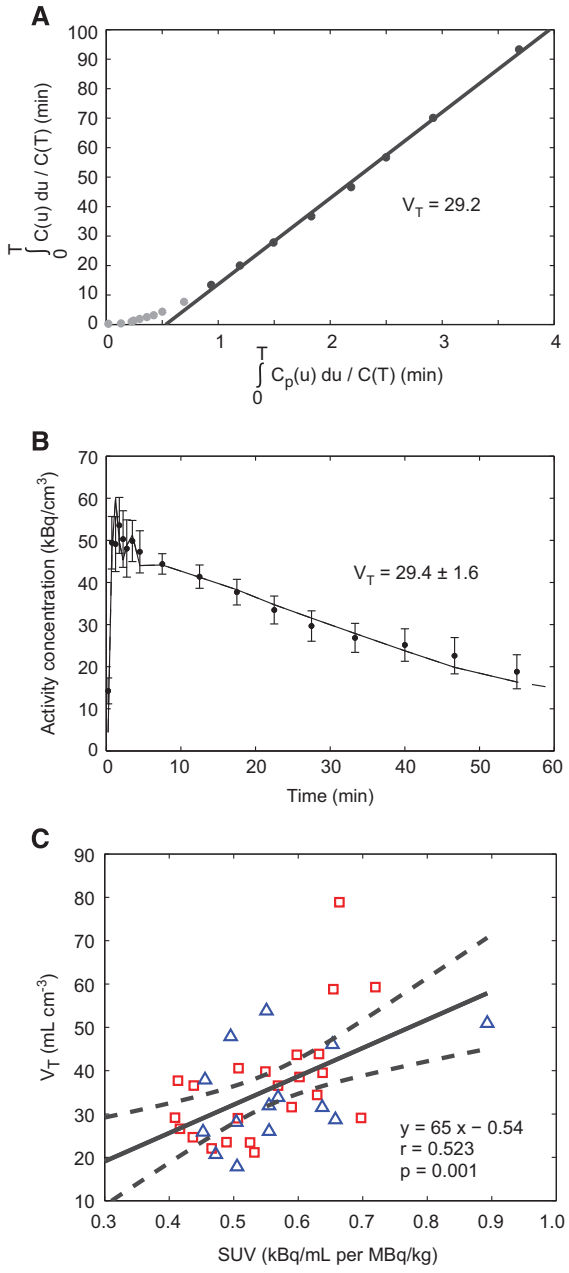

Figure 3. A representative example showing estimation of V_T for the whole-brain region, using metabolite-corrected arterial blood and positron emission tomography (PET) data collected from a transgenic rat aged 4 months, along with the correlation against standard uptake value (SUV). (**A**) Logan analysis. (**B**) Compartmental modeling using non-linear least squares (NLLS). (**C**) Comparison of SUV and V_T, where V_T was calculated using Logan analysis and SUV was calculated between 43 and 90 minutes. Red squares denote data from LRRK2 p.G2019S transgenic rats, with blue triangles denoting nontransgenic control rats.

without any significant interaction effects between genotype and the linear or quadratic terms of the model. The SUV increased by 56% in 12 months of aging (4 to 16 months), from 0.44 to 0.69 g/mL. V_T increased by 91% over the same 12 months, from 30 to 57 mL/cm^3. For both SUV and V_T, the curve that best described the age dependence was a quadratic. For the SUV, the coefficients of the polynomial, a_0, a_1, and a_2, were 0.28, 0.0015, and -1.37×10^{-6}, respectively (all with $P<0.01$). For V_T, the coefficients were 30.8, -0.030, and 1.72×10^{-4}, respectively, where a_1 was not significant and a_2 had trend significance ($P=0.064$).

Table 2 provides our primary outcome measures, V_T, and SUV, alongside BP_{ND}, for 4- and 10-month-old rats for the various brain regions. In isolation, the individual rate constants were not well identified. Considering the slopes of a linear regression of SUV with age, we found no significant regional variations in the rate of increase of SUV with age across various regions of brain parenchyma (cerebellum, thalamus, cortex, hippocampus, striatum, and whole brain). There was however a significantly higher rate of increased SUV with age in the pituitary gland (95% CI on slope being 0.60 to 0.95 g/mL per year, compared with 0.19 to 0.29 g/mL per year for the whole brain). Conversely, the highly variable SUV in the fourth ventricle increased with age at a lower rate, if at all (95% CI of 0 to 0.23 g/mL per year).

The *in vivo* binding of PBR28 in aged rats was prevented by presaturation of TSPO receptors using PK11195. Presaturation studies in two rats aged 1 year showed a reduction in V_T by about 90%, as shown in Figure 5. Administration of PK11195 led to a large increase in the concentration of PBR28 in arterial plasma in both rats. The total activity concentration in plasma at 1-hour post injection was fivefold higher than usual, without any significant changes in the rate of metabolism. Administration of DMSO alone had no obvious effects on the concentration in blood, but visual analysis of the images suggested some reductions in uptake in peripheral tissues and in the brain, and the measured whole-brain V_T (Rat 2 only) was at the lower end of the expected range.

DISCUSSION

The presented data show that PBR28 binding, and hence TSPO expression, is higher in the brain of aged rodents as compared with younger ones. We attribute this to microglial activation occurring during normal aging. Increases in TSPO were detectable using both *in vivo* and *in vitro* PBR28-based methods. We found no differences in PBR28 binding, over a wide age range, between nontransgenic rats and rats that overexpress LRRK2 p.G2019S. In addition, our data give credence to the use of SUV as a simple and relatively precise (compared with V_T) PET-based measure of microglial activation in the case of normal aging.

In neurodegenerative disease or corresponding animal models, we can expect a different neuroinflammatory phenotype compared with that found after an acute insult. Increased TSPO expression may be subtle and occur in microglia of differing levels of activation or in other cells of the parenchyma (e.g., reactive astrocytes). Furthermore, the SUV could be affected by age-related changes in the tracer metabolism or biodistribution that are unrelated to neuroinflammation. For these reasons, our investigation included both autoradiography measurements and PET measurements with arterial blood sampling in young and aged rats. The observation that both V_T and SUV increase with age by broadly similar levels provides some reassurance for the use of SUV. The discrepancy between these *in vivo* measures and those obtained by autoradiography was however unexpected. Possible explanations for these differences include *in vivo* competition with endogenous ligands, modification of the binding sites during the tissue preparation process, and/or high levels of low affinity binding. To confirm that the increase in V_T with age was caused by an increase in receptor binding, we performed presaturation studies in aged rats. These studies confirmed that almost all of the observed age-related increases in PBR28 V_T, and likely most of the increases in SUV, could be attributed to an increase in available binding sites. The *in vivo* specificity for this tracer has also been shown by others in the rat,[12] monkey,[4,33] and human.[34]

The increase in PBR28 uptake with age is in agreement with the expectations for a TSPO ligand designed to quantify microglial activation. Aging is known to lead to changes in the microglial phenotype with a shift toward a more activated state; the

Table 1. Regional analysis of [^{11}C]PBR28 binding in young (4.0 months) and aged (19.6 months) rats using *in vitro* autoradiography. The quoted errors are standard errors on the mean

	TSPO density (nmol/cc)				
Group	*Striatum*[a]	*Frontal cortex*	*Cerebellum*[a]	*Midbrain*	*Whole brain*[a]
Young, control rats ($n=4$)	19 ± 2	24 ± 3	42 ± 6	28 ± 5	33 ± 4
Young, LRRK2 p.G2019S rats ($n=4$)	26 ± 3	33 ± 4	46 ± 4	35 ± 3	38 ± 3
Aged, control rats ($n=4$)	30 ± 3	34 ± 5	53 ± 4	30 ± 2	41 ± 3
Aged, LRRK2 p.G2019S rats ($n=4$)	32 ± 2	34 ± 2	55 ± 1	32 ± 3	43 ± 1

[a]Denotes that aging effects are significant for this region ($P < 0.05$). Genotype was not a significant factor for any region.

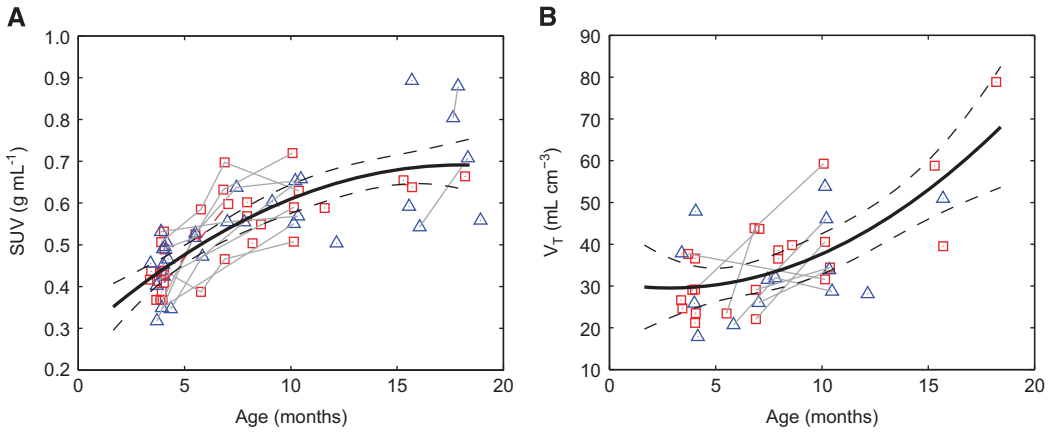

Figure 4. Effect of aging on [^{11}C]PBR28 uptake for the whole-brain region. (**A**) Aging effects on the standard uptake value (SUV). (**B**) Aging effects on V_T. In both graphs, the solid curve shows the quadratic model fit, with dashed curves indicating the 95% confidence limit for the fit. Lines join repeated scans in the same animal. Red squares denote data from LRRK2 p.G2019S transgenic rats, with blue triangles denoting non-transgenic control rats.

Table 2. Regional values for SUV, alongside results from kinetic modeling using NLLS, in rats aged 4 months and 10 months to show the effects of 6 months of aging

Metric and group	*Whole brain*	*Cerebellum*	*Thalamus*	*Cerebral cortex*	*Striatum*	*Pituitary gland*	*Fourth ventricle*
SUV (4 months old, $n=27$)	0.43 ± 0.01	0.45 ± 0.02	0.27 ± 0.01	0.37 ± 0.01	0.27 ± 0.01	1.47 ± 0.04	0.61 ± 0.04
SUV (10 months old, $n=12$)	0.59 ± 0.02	0.66 ± 0.03	0.46 ± 0.02	0.50 ± 0.01	0.41 ± 0.02	1.87 ± 0.07	0.73 ± 0.05
V_T (4 months old, $n=12$)	30 ± 3 (5%)	33 ± 3 (5%)	24 ± 2 (6%)	25 ± 2 (5%)	23 ± 2 (7%)	106[a] ± 16 (8%)	53 ± 9 (9%)
V_T (10 months old, $n=10$)	40 ± 4 (4%)	43 ± 3 (5%)	38 ± 4 (6%)	34 ± 3 (3%)	33 ± 3 (5%)	141 ± 18 (11%)	56 ± 7 (9%)
BP_{ND} (4 months old, $n=12$)	5.2 ± 1 (19%)	4.1 ± 1 (24%)	4.3 ± 1 (43%)	4.9 ± 1 (31%)	5.0 ± 1 (42%)	21[a] ± 5 (26%)	n.i.
BP_{ND} (10 months old, $n=10$)	7.3 ± 2 (19%)	6.1 ± 2 (21%)	5.1 ± 1 (32%)	7.7 ± 2 (16%)	4.8 ± 1 (37%)	24 ± 6 (19%)	n.i.

BP_{ND}, binding potential; n.i., not identifiable; NLLS, nonlinear least square; SUV, standard uptake value. The age ranges for the two groups are 3.4 to 4.4 and 8.6 to 12.1 months. Values are mean ± standard error on the mean. The parameter identifiability is given in parentheses as a percentage, calculated as the median value from the distribution of relative standard errors on the n parameter estimates. SUV has units of g/mL. V_T has units of mL/cm^3. [a]One outlying case was excluded for this region.

microglia tend to become larger and more complex, with several changes in antigen expression.[18,35–37]

Arterial blood sampling in rodents is technically challenging, and its requirement is not ideal for longitudinal investigations. The use of arterial blood data can also lead to additional variance in the outcome measures, seen here as a higher standard deviation in group-wise estimates and lower repeatability (ICC) for V_T as compared with blood-free measures (the SUV). The use of SUV as a blood-free measure to quantify [^{11}C]PBR28 PET data is an attractive approach, but only valid if these measurements are robust in their capacity to longitudinally track neuroinflammation in the rodent model (or human population) being studied. The data presented here suggest that the SUV might be useful in such investigations, but we advocate the collection of additional data to confirm the validity of the SUV in any particular model being studied. Although this study found little or no correlation between SUV and V_T after factoring out the aging effects (by considering the residual differences), the reduced data range of the residuals combined with the low precision of V_T measurements likely explains the lack of correlation.

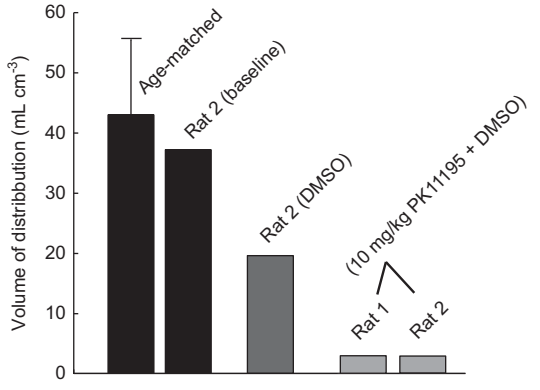

Figure 5. Results showing whole-brain V_T from presaturation studies in rats aged 1 year. The first bar gives the expected value for 1-year-old rats, with the standard deviation of the population indicated by the error bar. The second bar shows rat 2 imaged without intervention. The third bar gives V_T for rat 2 after injection of DMSO. The final two bars show V_T measured after presaturation with 10 mg/kg PK11195 dissolved in DMSO.

In various situations, the correspondence between SUV and V_T may be diminished, as was seen here in the case of presaturation studies using PK11195 where blockade of the peripheral binding site caused a large change in the concentration of circulating tracer. This change in the input function confounds the use of SUVs. In the two presaturation studies with DMSO+PK11195, the SUV was 0.38 and 0.40 for rats 1 and 2. These values are misleading if compared with the SUVs obtained with either DMSO alone (0.40 and 0.73 for rats 1 and 2) or baseline values (0.68 for rat 2, 0.65 for the model prediction). The SUV obtained in studies where large physiologic changes and changes in the concentration of tracer in blood occur (e.g., in blocking studies, possibly in the presence of disease, possibly after administration of DMSO) should hence not be used as a comparative measure of TSPO levels. In our aging study, we did assess the blood data for age-related changes, but found no correlation between age and the integral of the metabolite-corrected AIF between scan start and end times, and no correlation between age and the time taken for the parent fraction to drop to 0.5, which is supportive of SUV being a useful measure of the tracer's binding in this case. We also assessed the impact of changing the integration limits for SUV to 10 to 65 minutes, but found minimal changes in the observed aging relationship and measurement variability. Similarly, the sensitivity of the Logan-derived V_T estimate to the chosen start and end times for the linear regression was assessed. Only small changes ($< 4.5\%$) were observed in the mean value of the whole-brain V_T when changing the fitting range to 20 to 65 minutes or 10 to 80 minutes. as compared with the reference value calculated using the range 10 to 65 minutes.

Due to radiochemistry limitations, the specific activity of PBR28 at the time of injection for PET imaging had a wide range and introduced the possibility of effects related to the injected mass of PBR28. We examined the data for any systematic effect of the injected mass on SUV and V_T, but observed no significant relationships or strong trends. These data were however quite sparse near the limits of the injected mass range.

Partial volume effects, specifically the spill-in from the pituitary gland and ventricular regions, could contribute to the apparent increases in tracer uptake throughout the brain. Such effects are however unlikely to explain the strong age-related increases in uptake, because the SUV for the fourth ventricle had little or no dependence on age, and because the distance from the pituitary gland to regions such as the cerebellum (which showed large age-related increases) is several times the FWHM for the spatial resolution of the image.

Many assessments of age-related changes in TSPO levels in the human brain have been made using PET imaging, but findings have are mixed. Recent examples include the study by Kumar *et al*,[38] in which an increase in the SUV but not in the distribution volume ratio of PK11195, was observed with age. The study by Suridjan *et al*[39] did not find age-related changes in the binding of the second-generation TSPO ligand [^{18}F]-FEPPA. In this case, quantification was via V_T estimated using a metabolite-corrected arterial plasma input function for which, as in the current study, there was a large interindividual variability. In work by Gulyás *et al*,[40] the SUV of [^{11}C]vinpocetine was found to increase with age in some brain regions, with similar increases found for healthy controls and patients with Alzheimer's disease.

We conclude that the expression of TSPO, a marker of microglial activation, is increased in the aged rat brain as determined from *in vivo* PET and *in vitro* autoradiographic measures of PBR28 binding. We observed no difference in PBR28 binding between normal control rats compared with transgenic rats that over-express the PD-related p.G2019S mutated form of LRRK2, suggesting that this mutation does not exacerbate the microglial priming or activation that occurs with age.

DISCLOSURE/CONFLICT OF INTEREST

The authors declare no conflict of interest.

ACKNOWLEDGMENTS

The authors acknowledge the assistance from staffs at the UBC PET group and TRIUMF. Drs Doris Doudet and Steen Jakobsen provided valuable assistance with data interpretation and analysis of radiometabolites. Drs Robert Mach and Jinbin Xu provided assistance with the setup of [^{11}C]PBR28 production and autoradiography.

REFERENCES

1 Glass CK, Saijo K, Winner B, Marchetto MC, Gage FH. Mechanisms underlying inflammation in neurodegeneration. *Cell* 2010; **140**: 918–934.
2 Tansey MG, Goldberg MS. Neuroinflammation in Parkinson's disease: its role in neuronal death and implications for therapeutic intervention. *Neurobiol Dis* 2010; **37**: 510–518.
3 Perry VH, Holmes C. Microglial priming in neurodegenerative disease. *Nat Rev Neurol* 2014; **10**: 217–224.
4 Briard E, Zoghbi SS, Imaizumi M, Gourley JP, Shetty HU, Hong J *et al.* Synthesis and evaluation in monkey of two sensitive 11C-labeled aryloxyanilide ligands for imaging brain peripheral benzodiazepine receptors *in vivo*. *J Med Chem* 2008; **51**: 17–30.
5 Walker M, Dinelle K, Lee N, Adam M, Takhar C, Xu J *et al.* Quantification of inflammation in the rat brain using [11C]PBR28 PET. *J Nucl Med Meeting Abstracts* 2013; **54**: 1743.
6 Zimprich A, Biskup S, Leitner P, Lichtner P, Farrer M, Lincoln S *et al.* Mutations in LRRK2 cause autosomal-dominant parkinsonism with pleomorphic pathology. *Neuron* 2004; **44**: 601–607.
7 Paisan-Ruiz C, Jain S, Evans EW, Gilks WP, Simon J, van der BM *et al.* Cloning of the gene containing mutations that cause PARK8-linked Parkinson's disease. *Neuron* 2004; **44**: 595–600.
8 Rupprecht R, Papadopoulos V, Rammes G, Baghai TC, Fan J, Akula N *et al.* Translocator protein (18 kDa) (TSPO) as a therapeutic target for neurological and psychiatric disorders. *Nat Rev Drug Discov* 2010; **9**: 971–988.
9 Gavish M, Bachman I, Shoukrun R, Katz Y, Veenman L, Weisinger G *et al.* Enigma of the peripheral benzodiazepine receptor. *Pharmacol Rev* 1999; **51**: 629–650.
10 Casellas P, Galiegue S, Basile AS. Peripheral benzodiazepine receptors and mitochondrial function. *Neurochem Int* 2002; **40**: 475–486.
11 Banati RB. Visualising microglial activation *in vivo*. *Glia* 2002; **40**: 206–217.
12 Imaizumi M, Kim HJ, Zoghbi SS, Briard E, Hong J, Musachio JL *et al.* PET imaging with [11C]PBR28 can localize and quantify upregulated peripheral benzodiazepine receptors associated with cerebral ischemia in rat. *Neurosci Lett* 2007; **411**: 200–205.
13 Wilson AA, Garcia A, Parkes J, McCormick P, Stephenson KA, Houle S *et al.* Radiosynthesis and initial evaluation of [18F]-FEPPA for PET imaging of peripheral benzodiazepine receptors. *Nucl Med Biol* 2008; **35**: 305–314.

14 Boutin H, Prenant C, Maroy R, Galea J, Greenhalgh AD, Smigova A *et al.* [18F] DPA-714: direct comparison with [11C]PK11195 in a model of cerebral ischemia in rats. *PLoS ONE* 2013; **8**: e56441.
15 Ito F, Toyama H, Kudo G, Suzuki H, Hatano K, Ichise M *et al.* Two activated stages of microglia and PET imaging of peripheral benzodiazepine receptors with [(11)C] PK11195 in rats. *Ann Nucl Med* 2010; **24**: 163–169.
16 Venneti S, Lopresti BJ, Wang G, Hamilton RL, Mathis CA, Klunk WE *et al.* PK11195 labels activated microglia in Alzheimer's disease and *in vivo* in a mouse model using PET. *Neurobiol Aging* 2009; **30**: 1217–1226.
17 Drake C, Boutin H, Jones MS, Denes A, McColl BW, Selvarajah JR *et al.* Brain inflammation is induced by co-morbidities and risk factors for stroke. *Brain Behav Immun* 2011; **25**: 1113–1122.
18 Ogura K, Ogawa M, Yoshida M. Effects of ageing on microglia in the normal rat brain: immunohistochemical observations. *Neuroreport* 1994; **5**: 1224–1226.
19 Gillardon F, Schmid R, Draheim H. Parkinson's disease-linked leucine-rich repeat kinase 2(R1441G) mutation increases proinflammatory cytokine release from activated primary microglial cells and resultant neurotoxicity. *Neuroscience* 2012; **208**: 41–48.
20 Moehle MS, Webber PJ, Tse T, Sukar N, Standaert DG, DeSilva TM *et al.* LRRK2 inhibition attenuates microglial inflammatory responses. *J Neurosci* 2012; **32**: 1602–1611.
21 Walker MD, Volta M, Cataldi S, Dinelle K, Beccano-Kelly D, Munsie L *et al.* Behavioral deficits and striatal DA signaling in LRRK2 p.G2019S transgenic rats: a multimodal investigation including PET neuroimaging. *J Parkinsons Dis* 2014; **4**: 483–498.
22 Hoareau R, Shao X, Henderson BD, Scott PJ. Fully automated radiosynthesis of [(1)(1)C]PBR28, a radiopharmaceutical for the translocator protein (TSPO) 18 kDa, using a GE TRACERlab FXC-Pro. *Appl Radiat Isot* 2012; **70**: 1779–1783.
23 Leaver KR, Reynolds A, Bodard S, Guilloteau D, Chalon S, Kassiou M. Effects of translocator protein (18 kDa) ligands on microglial activation and neuronal death in the quinolinic-acid-injected rat striatum. *ACS Chem Neurosci* 2012; **3**: 114–119.
24 Kim JS, Lee JS, Im KC, Kim SJ, Kim SY, Lee DS *et al.* Performance measurement of the microPET focus 120 scanner. *J Nucl Med* 2007; **48**: 1527–1535.
25 Brown C. Blood collection from the tail of a rat. *Lab Animal* 2006; **35**: 24–25.
26 Rubins DJ, Melega WP, Lacan G, Way B, Plenevaux A, Luxen A *et al.* Development and evaluation of an automated atlas-based image analysis method for microPET studies of the rat brain. *Neuroimage* 2003; **20**: 2100–2118.
27 Logan J, Fowler JS, Volkow ND, Wolf AP, Dewey SL, Schlyer DJ *et al.* Graphical analysis of reversible radioligand binding from time-activity measurements applied to [N-11C-methyl]-(-)-cocaine PET studies in human subjects. *J Cereb Blood Flow Metab* 1990; **10**: 740–747.
28 Walker MD, Matthews JC, Asselin MC, Watson CC, Saleem A, Dickinson C *et al.* Development and validation of a variance model for dynamic PET: uses in fitting kinetic data and optimizing the injected activity. *Phys Med Biol* 2010; **55**: 6655–6672.
29 Innis RB, Cunningham VJ, Delforge J, Fujita M, Gjedde A, Gunn RN *et al.* Consensus nomenclature for *in vivo* imaging of reversibly binding radioligands. *J Cereb Blood Flow Metab* 2007; **27**: 1533–1539.
30 Tellinghuisen J. Statistical error propagation. *J Phys Chem A* 2001; **105**: 3917–3921.
31 Strome EM, Jivan S, Doudet DJ. Quantitative *in vitro* phosphor imaging using [3H] and [18F] radioligands: the effects of chronic desipramine treatment on serotonin 5-HT2 receptors. *J Neurosci Methods* 2005; **141**: 143–154.
32 Maia S, Arlicot N, Vierron E, Bodard S, Vergote J, Guilloteau D *et al.* Longitudinal and parallel monitoring of neuroinflammation and neurodegeneration in a 6-hydroxydopamine rat model of Parkinson's disease. *Synapse* 2012; **66**: 573–583.
33 Imaizumi M, Briard E, Zoghbi SS, Gourley JP, Hong J, Fujimura Y *et al.* Brain and whole-body imaging in nonhuman primates of [11C]PBR28, a promising PET radioligand for peripheral benzodiazepine receptors. *Neuroimage* 2008; **39**: 1289–1298.
34 Owen DR, Guo Q, Kalk NJ, Colasanti A, Kalogiannopoulou D, Dimber R *et al.* Determination of [(11)C]PBR28 binding potential *in vivo*: a first human TSPO blocking study. *J Cereb Blood Flow Metab* 2014; **34**: 989–994.
35 Viana LC, Lima CM, Oliveira MA, Borges RP, Cardoso TT, Almeida IN *et al.* Litter size, age-related memory impairments, and microglial changes in rat dentate gyrus: stereological analysis and three dimensional morphometry. *Neuroscience* 2013; **238**: 280–296.
36 Perry VH, Matyszak MK, Fearn S. Altered antigen expression of microglia in the aged rodent CNS. *Glia* 1993; **7**: 60–67.
37 Hart AD, Wyttenbach A, Perry VH, Teeling JL. Age related changes in microglial phenotype vary between CNS regions: grey versus white matter differences. *Brain Behav Immun* 2012; **26**: 754–765.
38 Kumar A, Muzik O, Shandal V, Chugani D, Chakraborty P, Chugani HT. Evaluation of age-related changes in translocator protein (TSPO) in human brain using (11)C-[R]-PK11195 PET. *J Neuroinflammation* 2012; **9**: 232.
39 Suridjan I, Rusjan PM, Voineskos AN, Selvanathan T, Setiawan E, Strafella AP *et al.* Neuroinflammation in healthy aging: a PET study using a novel Translocator Protein 18kDa (TSPO) radioligand, [(18)F]-FEPPA. *Neuroimage* 2014; **84**: 868–875.
40 Gulyas B, Vas A, Toth M, Takano A, Varrone A, Cselenyi Z *et al.* Age and disease related changes in the translocator protein (TSPO) system in the human brain: positron emission tomography measurements with [11C]vinpocetine. *Neuroimage* 2011; **56**: 1111–1121.